A&A 391, 1005–1012 (2002)
DOI: 10.1051/0004-6361:20020846

Astronomy & Astrophysics

Pulsating or not? A search for hidden pulsations below the red edge of the ZZ Ceti instability strip⋆

R. Kotak[1], M. H. van Kerkwijk[2], J. C. Clemens[3,⋆⋆], and T. A. Bida[4]

[1] Lund Observatory, Box 43, 22100 Lund, Sweden
[2] Astronomical Institute, Utrecht University, PO Box 80000, 3508 TA Utrecht, The Netherlands
e-mail: M.H.vanKerkwijk@astro.uu.nl
[3] Department of Physics and Astronomy, University of North Carolina, Chapel Hill, NC 27599-3255, USA
e-mail: clemens@physics.unc.edu
[4] Lowell Observatory, 1400 W Mars Hill Rd., Flagstaff, AZ 86001, USA
e-mail: tbida@lowell.edu

Received 3 April 2002 / Accepted 4 June 2002

Abstract. The location of the red edge of the ZZ Ceti instability strip is defined observationally as being the lowest temperature for which a white dwarf with a H-rich atmosphere (DA) is known to exhibit periodic brightness variations. Whether this cut-off in flux variations is actually due to a cessation of pulsation or merely due to the attenuation of any variations by the convection zone, rendering them invisible, is not clear. The latter is a theoretical possibility because with decreasing effective temperature, the emergent flux variations become an ever smaller fraction of the amplitude of the flux variations in the interior. In contrast to the flux variations, the visibility of the velocity variations associated with the pulsations is not thought to be similarly affected. Thus, models imply that were it still pulsating, a white dwarf just below the observed red edge should show velocity variations. In order to test this possibility, we used time-resolved spectra of three DA white dwarfs that do not show photometric variability, but which have derived temperatures only slightly lower than the coolest ZZ Ceti variables. We find that none of our three targets show significant periodic velocity variations, and set 95% confidence limits on amplitudes of 3.0, 5.2, and 8.8 km s^{-1}. Thus, for two out of our three objects, we can rule out velocity variations as large as 5.4 km s^{-1} observed for the strongest mode in the cool white dwarf pulsator ZZ Psc. In order to verify our procedures, we also examined similar data of a known ZZ Ceti, HL Tau 76. Applying external information from the light curve, we detect significant velocity variations for this object with amplitudes of up to 4 km s^{-1}. Our results suggest that substantial numbers of pulsators having large velocity amplitudes do not exist below the observed photometric red edge and that the latter probably reflects a real termination of pulsations.

Key words. stars: white dwarfs – stars: oscillations – convection

1. Introduction

In spite of advances in theoretical formulations and observational capabilities, the details of the inner workings of the cool H-rich pulsating white dwarfs (DAVs or ZZ Cetis) continue to elude us.

Early attempts to explain the nature of the driving of the pulsations of ZZ Cetis postulated that driving occurred via the κ-mechanism – i.e. in a manner akin to that in Cepheids and δ-Scuti stars – (e.g. Dolez & Vauclair 1981; Dziembowski & Koester 1981; Winget et al. 1982) thereby ignoring the effects of pulsation on the convection zone (also known as the "frozen-in" approximation) even though radiative flux transport is negligible in these regions. Brickhill (1991) realised that the response of the convection zone to the perturbation is almost instantaneous (∼1 s) compared to the periods of the g-modes (hundreds of seconds). He found that as a result, the convection zone itself can drive the pulsations: part of the flux perturbations entering the convection zone from the largely radiative interior are absorbed by the convection zone and are released half a cycle later. This interaction between the perturbation and the response of the convection zone drives the g-modes.

Within the framework of this "convective-driving" mechanism, recently confirmed analytically by Goldreich & Wu (1999a), the blue edge of the instability strip i.e. the hottest temperature for which pulsations are excited and at which pulsations are expected to be observable, is set by the condition that $\omega\tau_c \approx 1$ for radial order, $n = 1$ and spherical degree $\ell = 1$; ω is the radian frequency and τ_c the thermal time constant of

Send offprint requests to: R. Kotak, e-mail: rubina@astro.lu.se

⋆ The data presented herein were obtained at the W. M. Keck Observatory, which is operated as a scientific partnership among the California Institute of Technology, the University of California and the National Aeronautics and Space Administration. The Observatory was made possible by the generous financial support of the W. M. Keck Foundation.

⋆⋆ Alfred P. Sloan Research Fellow.

the convection zone. (Note that τ_c is different from the "global" thermal time scale, t_t in Brickhill 1991. Where necessary, we follow the notation of Goldreich & Wu 1999a.)

The location of the red edge is less clearly defined. As long as a mode is driven, its intrinsic amplitude is likely to remain roughly constant as it is most likely set by parametric resonance with stable daughter modes (Wu & Goldreich 2001). As the white dwarf cools, the depth of the convection zone increases, and damping in the shear layer at the base of the convection zone becomes stronger. At some stage, damping will exceed the driving due to the convection zone. This sets the physical red edge, beyond which pulsations are no longer excited.

Observationally, though, the red edge may appear at *higher* temperatures. This is because, as the convection zone deepens, the amplitude of flux variations at the photosphere becomes an ever smaller fraction of the amplitude in deeper layers; the convection zone acts as a low-pass, frequency-dependent filter leading to a reduction in flux given by (Goldreich & Wu 1999a)

$$\left(\frac{\Delta F}{F}\right)_{\rm ph} = \left(\frac{\Delta F}{F}\right)_{\rm b} \frac{1}{\sqrt{1+(\omega\tau_c)^2}} \quad (1)$$

where the subscripts "ph" and "b" refer to the photospheric flux variation and that at the base of the convection zone respectively, for a particular eigenmode. From Eq. (1) one expects that the observed amplitude of a given mode will decrease smoothly with increasing τ_c, and thus with decreasing temperature. This might seem inconsistent with the observations, which show a rather sharply defined red edge. However, τ_c depends very steeply on temperature, and hence it may also be that the observations do not yet resolve the transition from easily to barely visible (see Fig. 8 in Wu & Goldreich 1999).

Given the uncertainties in the physical processes leading to damping, it is not clear whether the observed red edge corresponds to the physical red edge, or whether it is just an apparent red edge where pulsations are still driven, but do not give rise to observable flux variations at the photosphere. The implication, then, is that a perfectly constant white dwarf might actually still be pulsating!

Theoretical uncertainties aside, there are also uncertainties in interpreting the observations. Indeed, over the years, the location and extent of the observed ZZ Ceti instability strip have undergone several transformations (e.g., Greenstein 1982; Robinson et al. 1995; Giovannini et al. 1998). This is due in part to the difficulty in accurately determining the atmospheric parameters of objects having convectively unstable atmospheres, as some version of the mixing length prescription usually has to be assumed. Additionally, at optical wavelengths, the Balmer lines attain their maximum strengths close to the instability strip. The unfortunate consequence is that varying the atmospheric parameters gives rise to only slight changes in the appearance of the spectra, making it difficult to uniquely fit observed spectra (e.g., Koester & Vauclair 1996). Supplementary constraints in the form of *uv* spectra, parallaxes, gravitational redshifts, have almost become a prerequisite.

Most studies to date have only considered flux variations. However, velocity variations are necessarily associated with these flux variations and though small – of the order of a few km s^{-1} – have nevertheless been measured in ZZ Ceti white dwarfs: securely in ZZ Psc (van Kerkwijk et al. 2000), and probably also in HS 0507+0434B (Kotak et al. 2002). That there are negligible vertical velocity gradients in the convection zone due to damping by turbulent viscosity is a central tenet of the convective-driving theory (Brickhill 1990; Goldreich & Wu 1999b). Indeed for shallow convection zones, this simplification has been shown to hold in the 2D hydrodynamical simulations of Gautschy et al. (1996). This means that the horizontal velocity is nearly *independent* of depth in the convection zone so that although photometric variations become difficult to detect around the red edge of the instability strip as mentioned above, velocity variations pass virtually undiminished through the convection zone.

Observationally, the consequence would be that the putative, perfectly constant white dwarf might reveal its pulsating nature by velocity variations. If objects below the red edge follow the same trend as the known pulsators i.e. longer pulsation periods and higher amplitudes with decreasing effective temperature (Clemens 1993), then we expect the highest velocity amplitudes at the longer ($\gtrsim$600 s) periods. For ZZ Psc (a.k.a. G 29–38), a well-known pulsator close to the red edge, van Kerkwijk et al. (2000) measured a velocity amplitude of 5.4 km s^{-1} for the strongest mode at 614 s. For all our objects, which are cooler, we expect velocity amplitudes at least as large as those measured for ZZ Psc – lower values would constitute a non-detection.

Armed with this testable theoretical expectation, we look for variations in the line-of-sight velocities in objects that lie just below the photometric red edge of the instability strip. Our three targets are chosen – subject to visibility constraints during the scheduled run – from the list of Kepler et al. (1995) who find a handful of non-pulsating ZZ Cetis close to the red edge of the instability strip. Kepler et al. (1995) inferred relatively high masses for two of our three targets (see Table 1). This inference, though dependent on the assumed convective prescription, would imply that these objects have instability strips at higher temperatures.

In addition to the above, we search for line-of-sight velocity variations in the first ZZ Ceti to be discovered, HL Tau 76 (Landolt 1968), using exactly the same instrumental setup and reduction techniques so that it serves as a comparison case. Treating it subsequently as a ZZ Ceti variable (Appendix A) allows us to indirectly constrain the spherical degree of the eigenmodes.

2. Observations and data reduction

Time-resolved spectra of three alleged non-pulsators, G 1–7, G 67–23, and G 126–18 (Kepler et al. 1995) and one known ZZ Ceti-type white dwarf, HL Tau 76, were acquired using the Low Resolution Imaging Spectrometer (Oke et al. 1995) on the Keck II telescope during a service run on the nights of 18th and 20th October 1997. In addition to the above, we took time-resolved spectra of G 126–18 during an observing run with the same instrument and set-up on 11th December 1997. Details of the observations together with other quantities are

Table 1. Observations.

	WD number	$T_{\rm eff}$ (K)	$\log g$	V	Start UT	End UT	Exposure Time (s)	No. of frames	Scatter (km s^{-1})	Measurement error (km s^{-1})
HL Tau 76 (s)	0416 + 272	11 440	7.89 ± 0.05	15.2	12:58:55	14:59:06	20	213	9.0	6.7
G 1–7 (s)	0033 + 013	11 214	8.70 ± 0.06	15.5	08:37:49	10:39:50	74	83	9.8	7.7
G 67–23 (s)	2246 + 223	10 770	8.78 ± 0.03	14.4	07:33:57	08:48:15	74	50	3.5	2.4
G 126–18	2136 + 229	10 550	8.17 ± 0.05	15.3	04:46:06	06:27:25	30	136	1.4	7.6
G 126–18 (s)					06:58:18	08:58:03	74	80	5.2	4.0

Note. The effective temperature and $\log g$ for each of the 3 red edge objects are taken from Kepler et al. (1995) and are inferred from optical data only using the ML2, $\alpha = 1$ prescription for describing the convective flux. For HL Tau 76, these quantities are taken from Bergeron et al. (1995) and are constrained using both *uv* and optical spectra for ML2/$\alpha = 0.6$. The scatter due to wander is calculated at a representative wavelength of 4341 Å i.e. at Hγ. The measurement error is the typical internal error on the line-of-sight velocity associated with the fits to the line profiles as described in Sect. 4. "(s)" refers to the Oct. 1997 service run data. The number of frames refers to the number of *useful* frames.

summarized in Table 1. An 8.″7 slit was used with a 600 line mm^{-1} grating, the resulting dispersion being ∼1.25 Å pix^{-1}. For the service run, the seeing was around 1.″0, yielding a resolution of 6 Å, while the December 1997 data were taken in slightly worse seeing conditions (1.″2), corresponding to a resolution of about 7 Å. A problem with the Active Control System meant that 22 frames of G 67–23 taken during the beginning of the run had to be discarded and 4 frames taken at the very end of the run also had to be disregarded as the position of the target in the slit seemed to have altered. The last frame of HL Tau 76 was not used as it was clear that light was being lost. For the observations taken during the service run, we were unfortunately unable to obtain a sufficient number of halogen frames so we decided to forgo flatfielding the spectra altogether.

Shifts in the positions of the Balmer lines are introduced by instrumental flexure and differential atmospheric refraction. As in van Kerkwijk et al. (2000), we corrected for the former using the position of the O I λ 5577 Å sky emission line, and for the latter by computing the wavelength-dependent shifts using the recipe of Stone (1996). As the spectra were taken through a wide slit, the positions of the Balmer lines will also depend on the exact position of the target in the slit. In principle, this position should be tied to the position of the guide star, but in practice we found that there was substantial random jitter, probably due to guiding errors and differential flexure between the guider and the slit.

One way of accounting for the random movements in the slit is to in effect "tag" the movements of the target to those of a reference star that can also be accommodated in the slit. For the Dec. 1997 observations, the slit was set at a position angle such that a G-type star was in the slit together with G 126–18. The wandering of G 126–18 could then be corrected for using the positions of Hβ of the former as fiducial points.

An estimate of the scatter due to random wander in the slit can be obtained by measuring the shifts along the slit of the spatial profiles and translating these into scatter in the dispersion direction. To do this, we simply fit Gaussian functions to the spatial profiles, and fit a low order polynomial to the resulting centroid positions (if no reference star was available). The standard deviation of the centroid positions from the smooth curve is then a proxy of the scatter due to wander in the slit. We compute this scatter at the representative wavelength of Hγ. The resulting estimates are shown in Table 1. As expected, the use of a reference object for G 126–18 dramatically lowers the scatter in the measured line-of-sight velocities (see Table 1). However, the value for G 67–23 shows that commensurate results can also be obtained without a local calibrator if the observing conditions and guiding are sufficiently stable.

3. Lightcurves

Lightcurves for all objects were constructed by dividing the line-free region of the continuum between ∼5300–5700 Å by the average of that region. The Fourier transforms of the light curves were calculated up to the Nyquist frequency and are shown in Fig. 1. No clear periodicities are evident for G 67–23, G 1–7, and G 126–18, as expected based on the limits of 0.25%, 0.37%, and 0.46% respectively set by Kepler et al. (1995).

4. Line of sight velocities

Velocity curves were constructed by measuring the Doppler shifts of three Balmer lines: Hβ, Hγ, and Hδ. This was done by fitting a sum of a Gaussian and Lorentzian profile and approximating the continuum by a line. The centroids of the Gaussian and Lorentzian functions were forced to be the same. The wavelength intervals chosen for our fits were ∼388 Å, 300 Å, and 164 Å centred approximately on Hβ, Hγ, and Hδ respectively. We computed the velocity curve by simply averaging the velocities derived from each line.

The measurement errors are of the order of the scatter due to random wander in all but one of the series of spectra (Table 1). The one exception is the series taken of G 126–18 in Dec. 1997, where the scatter is much smaller because of the tie to a reference object. Our measurements are most precise for G 67–23. We include our estimates for the scatter due to random wander in the least squares fit of the velocity curve (see below); the resulting fits all have $\chi^2_{\rm red} \simeq 1$.

The Fourier Transforms of the velocity curves are shown in Fig. 1. None of the red edge objects show a clear peak well above the noise level at any frequency.

For HL Tau 76, two of the stronger peaks have corresponding peaks in the light curve. However, there are also two other peaks evident in Fig. 1 at 6651 μHz and 6928 μHz that are not present in the light curve at amplitudes greater than 0.9 ± 0.8%

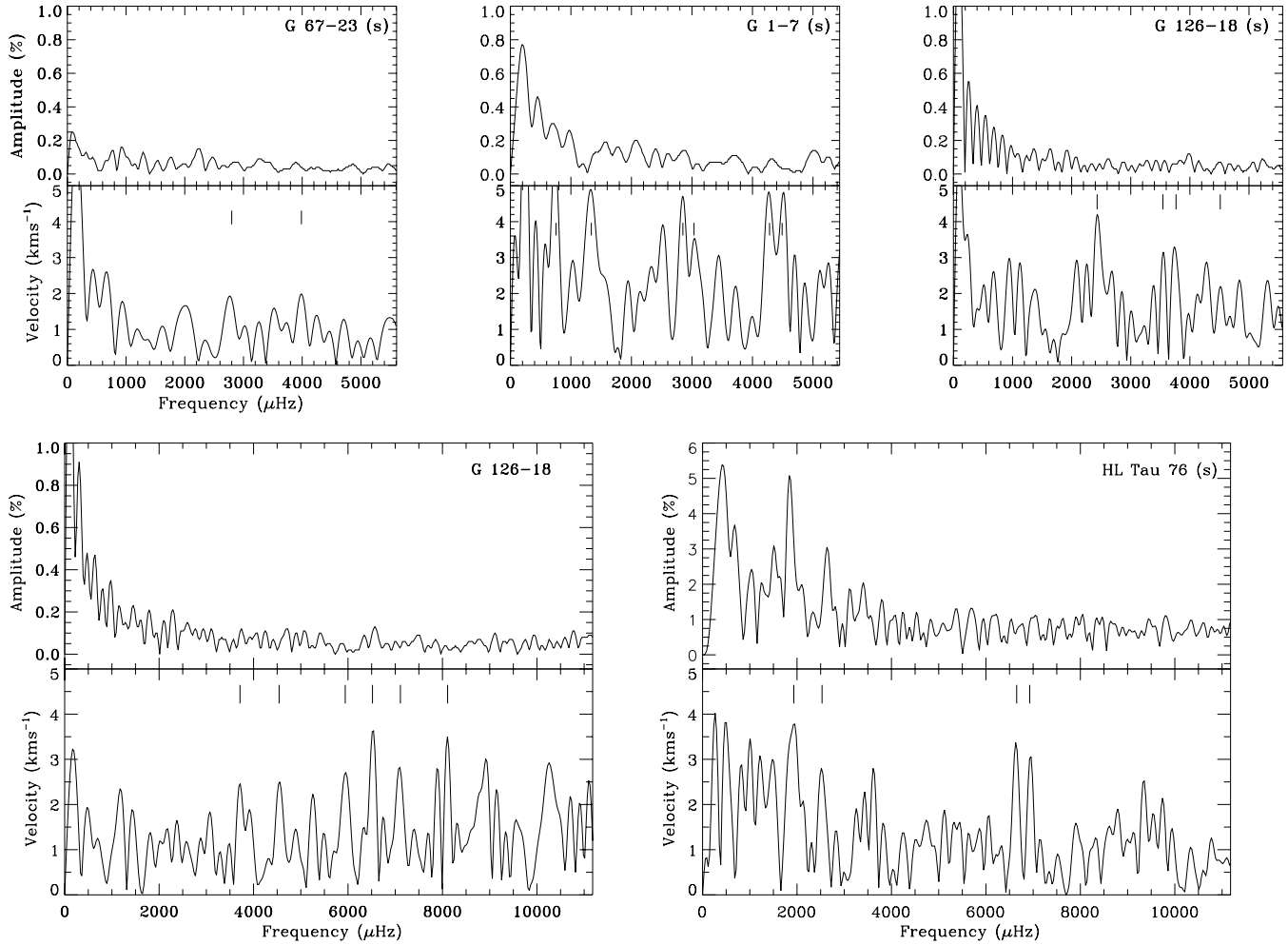

Fig. 1. Fourier transforms of the light (top panels) and velocity curves (bottom panels) for all objects. The marked peaks have been included in the Monte Carlo simulations in Sect. 4.1. We find no significant peaks in either the flux or the velocity FTs for G 1–7, G 126–18, and G 67–23. All FTs are shown up to the Nyquist Frequency except that of HL Tau 76 for clarity (see also caption to Fig. A.1).

and $0.6 \pm 0.8\%$ respectively i.e. well below our detection limit. We will return to this point in Appendix A.

Although it is clear from Fig. 1 that none of our objects show a large ($\gtrsim$5 km s^{-1}) peak at any frequency, given the disparities in the quality of our various data sets we must carry out tests in order to be able to place meaningful limits. We describe below two different Monte Carlo tests we devised to obtain quantitative estimates.

4.1. Significance of possible detections

We first looked for periodicities in each of the velocity curves by concentrating on the few peaks of relatively high amplitude in the Fourier transform of the velocity curves and fitting these successively with sinusoids, the frequencies, amplitudes, and phases all being free parameters. We included a low order polynomial in the fit to remove slow variations for all objects except G 126–18 (Dec. 1997) for which the calibration with respect to the reference star will have already removed any slow variations.

The first test we carry out aims to determine the likelihood of the peaks seen in the Fourier Transforms (Fig. 1) as being simply due to random noise. We shuffle the measured velocities randomly with respect to their measurement times after removing slow variations by fitting a 3rd-order polynomial for all objects (except G 126–18, Dec. 1997). We then determine the amplitude of the highest peak in the Fourier transform at any frequency between 700 μHz up to the Nyquist frequency. (This choice reflects an extended ZZ Ceti period range.) We repeat this procedure 1000 times, counting the number of artificial data sets in which the highest peak exceeded our maximum measured A_V. The higher this number, the higher the chance that even the strongest peak is not genuine. Table 2 shows our results. The strongest peaks in all the red edge objects can be attributed to noise. Only in HL Tau 76, the one known pulsator, is there an indication that the velocity signal is real. We show in Appendix A that external information (from the light curve) is necessary to confirm this.

Our second objective is to determine the minimum velocity amplitude in each data set for which we could have had a high ($\gtrsim$95%) degree of confidence that, had such a signal been present, we would have detected it. To do this, we inject an artificial signal in our data of a given amplitude and random frequency and phase. The random frequencies are chosen

Table 2. Results from Monte Carlo simulations of velocity amplitudes.

Object	Largest Peak in F.T. ν (μHz)	A_V (km s^{-1})	$P(>A_V)$ (%)	Detection Limit (~95%) (km s^{-1})
G 1–7 (s)	753	6.0 ± 1.5	42	8.8
G 126–18	6518	3.4 ± 1.0	67	5.2
G 126–18 (s)	2430	4.1 ± 1.2	35	5.9
G 67–23 (s)	3988	2.0 ± 0.7	60	3.0
HL Tau 76 (s)	1933	4.1 ± 1.0	17	5.1

Note. A_V is the maximum measured velocity amplitude for each object at the frequency (ν) specified in the first column. $P(>A_V)$ is the percentage probability that the largest peak (i.e. of amplitude A_V) is present solely by chance. The third column lists the velocity amplitude necessary to constitute a detection at the 95% confidence level – at any frequency – as estimated from our second Monte Carlo test (see also Fig. 2). Note that the frequency corresponding to the maximum velocity peak is different for the two G 126–18 data sets.

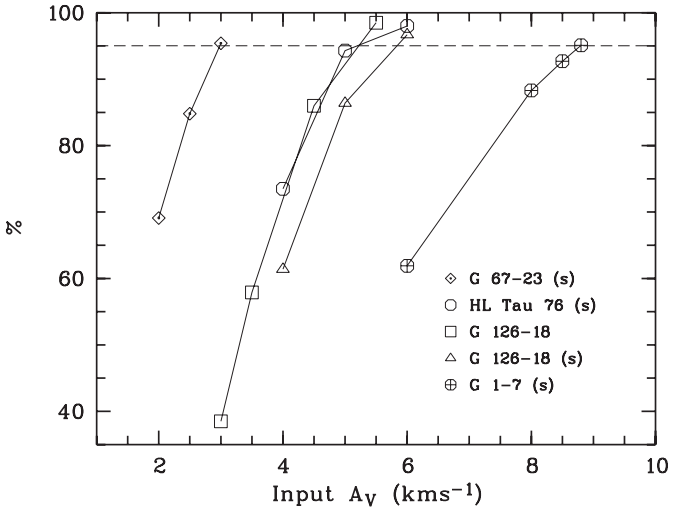

Fig. 2. Probabilities that the velocity signals with the given amplitudes that would have been detected in the different data sets had they been present. The dashed line shows the 95% confidence level, at or above which measured velocities would be taken to be significant. For our best data set (G 67–23), we can exclude periodic signals with amplitudes greater than 3 km s^{-1} with 95% confidence.

from 700 μHz up to the Nyquist frequency, while the phases are chosen from 0 to 2π. We repeat the procedure 1000 times and count the number of artificial data sets in which the highest peak in the Fourier transform is located within a range corresponding to the input random frequency plus or minus the frequency resolution of the data. We repeat the procedure, varying the input amplitude, until we recover the artificial peak as the maximum peak in at least 95% of the trials within the expected frequency range. We expect that the velocity amplitude we obtain in this manner will be somewhat higher than the detection limit derived above. This is because for peaks having an amplitude exactly at the detection limit, there is an equal chance of a noise peak either enhancing or diminishing it. Thus for a peak exactly at the detection limit, we cannot expect >50% confidence. This test implicitly assumes that none of the signal in our Fourier transform is real. For HL Tau 76, we show in the appendix that the higher peaks in the velocity Fourier Transform that are coincident with peaks in the Fourier Transform of the light curve are real. Hence, the limits for any signal not associated with flux variations will be slightly lower than those inferred from Fig. 2.

The results of the above simulation are displayed in Fig. 2. We can rule out velocity amplitudes larger than 5.4 km s^{-1} – as detected by van Kerkwijk et al. (2000) for ZZ Psc – for all objects except G 1–7. Our best limit for a minimum significant amplitude (3 km s^{-1}) comes from G 67–23.

5. Discussion and conclusions

We have analysed velocity curves of three white dwarfs below the photometric red edge of the instability strip to check whether the observed red edge corresponds to the physical one. For ZZ Psc, a white dwarf close to the red edge but still within the instability strip, van Kerkwijk et al. (2000) found a maximum velocity amplitude of 5.4 ± 0.8 km s^{-1}. We had expected larger modulations but for two objects we can exclude the presence of signals as strong as those in ZZ Psc with high confidence; for one of these two, G 67–23, we can exclude the presence of any signal greater than 3 km s^{-1}.

The above indicates that pulsations actually cease below the observed red edge. How secure is this conclusion? We see three weaknesses. The first is that in principle, destructive beating between different components in a multiplet might conceal a real signal in our short data sets. This, however, would be unlikely if multiple real signals were present. Furthermore, two data sets for the same object (G 126–18) taken during different observing runs are unlikely to be adversely affected. Two of the modulations found in G 126–18 (viz. 220 s and 269 s) seemed to be consistent with being at the same frequency and of the same amplitude – within the errors – for the two different observing runs. We carried out further Monte Carlo simulations to determine the likelihood of finding relatively strong peaks at the same frequency in two separate data sets. On the basis of these simulations, we conclude that these peak coincidences are almost certainly due to chance: even for the best case, the peaks at 265 s and 269 s, there is a 7% probability of a chance coincidence.

The second weakness is that our sensitivity turned out to be more marginal than we had hoped. We included one known ZZ Ceti, HL Tau 76, in the sample. Treating it as a red-edge object afforded a check on our methods. However, even for this bona-fide pulsator, we found that the velocity curve on its own was not sufficient to demonstrate velocity variations. A hint of a real signal was present, but this could only be confirmed by imposing external information from the light curve, information we lacked for the red-edge objects. In the process, HL Tau 76 was added to the select group of ZZ Cetis for which velocity variations have been detected.

The above might suggest that our experiment was simply not sensitive enough. One has to keep in mind however, that for the different objects rather different sensitivities were

reached. For one object, G 67–23, we can exclude the presence of velocity amplitudes as small as $3\,\mathrm{km\,s^{-1}}$ i.e. even smaller than the $4\,\mathrm{km\,s^{-1}}$ peak corresponding to strongest mode in HL Tau 76. Furthermore, on theoretical grounds alone, a velocity amplitude somewhat smaller than that of ZZ Psc is expected for HL Tau 76 given that it has a slightly higher temperature and its strongest mode, a slightly shorter period. This expectation is supported by the fact that the velocity amplitude of the dominant mode is in turn larger than that found for HS 0507+0434B, which is somewhat hotter still and has an even shorter dominant periodicity. On the same grounds, one would expect, as mentioned earlier, the red-edge objects to have larger velocity amplitudes than those observed in ZZ Psc, which, if present, would have been seen in two of the three objects[1].

The third weakness is perhaps the most severe: G 1–7 and G 67–23 have relatively high inferred masses, which implies that these objects would have ceased to be pulsationally active at a higher effective temperature than that expected for a typical $0.6\,M_{\odot}$ white dwarf, and are therefore not that close anymore to the red edge. At the same time, G 126–18, which has a normal mass, is the coolest of our three observed targets. Note though that the derived effective temperatures and surface gravities depend on the treatment of convection.

In summary, while not ironclad, our results indicate that pulsations have actually ceased below the observed red edge rather than having become photometrically undectable, and that the theoretical expectation of an extended instability strip, beyond the observed red edge is flawed. In order to settle the issue observationally, more sensitive measurements on objects closer to the red edge would be worthwhile; theoretically, detailed hydrodynamic modelling might go some way towards understanding the interplay of the various physical processes in defining the red edge.

Acknowledgements. We thank the referee, Detlev Koester, for his comments, and are grateful to Y. Wu for answering our many questions. R.K. would also like to thank J. S. Vink for encouragement and H-G. Ludwig for useful discussions. We also acknowledge support for a fellowship of the Royal Netherlands Academy of Arts and Sciences (MHvK) and partial support from the Knut och Alice Wallenbergs Stiftelse (RK). This research has made use of the SIMBAD database, operated at CDS, Strasbourg, France.

Appendix A: HL Tau 76

The Fourier Transform of the light curve of HL Tau 76 is characteristic of that of the ZZ Cetis (Fig. A.1). We fit the dominant peaks in the Fourier transform successively with a function of the form $A\cos(2\pi ft' - \phi) + C$ where A is the amplitude, f the frequency, ϕ the phase, and C, a constant offset. In order to reduce the covariance between the amplitudes and phases, the time axis is computed relative to the the middle of the time series ($t' = t - 13{:}59{:}01.56$ UT). We fixed the frequencies to those listed by Dolez & Kleinman (1996) in their preliminary analysis of WET (Whole Earth Telescope; Nather et al. 1990) data as these should be more reliable than the frequencies inferred from our data set, which only covers a short time span. We include all potential real modes listed in Table 4 of Dolez & Kleinman (1996) with an amplitude ≥0.9% except for modes at frequencies below $\sim 1000\,\mu$Hz as this corresponds to the noisiest region of our Fourier transform. The relevant quantities are listed in Table A.1. We find that our measured amplitudes (A_{L}) are on average 1% higher than those from the WET analysis.

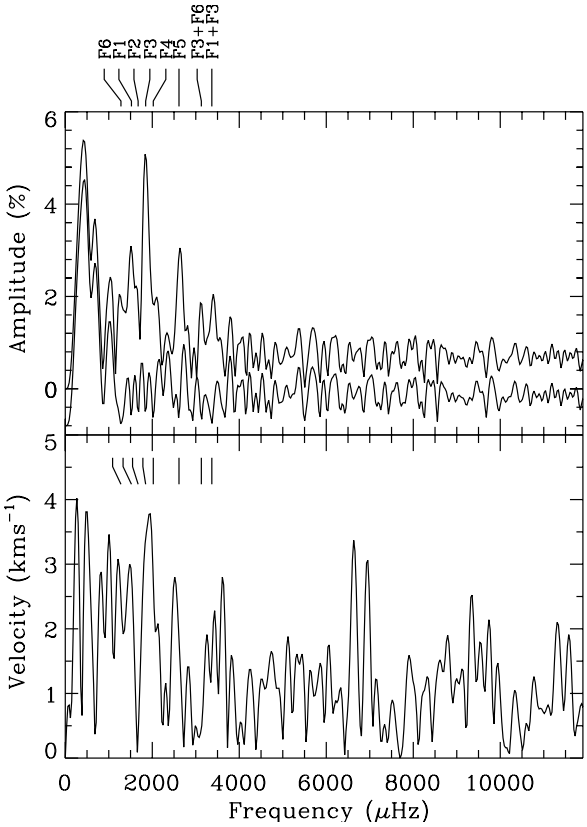

Fig. A.1. Fourier transform of the light curve **a)** and **b)** of the line-of-sight velocity variations shown up to 11 900 μHz for HL Tau 76. There are no peaks greater than 1% and $2.5\,\mathrm{km\,s^{-1}}$ longward of $11900\,\mu$Hz for **a)** and **b)** respectively. The lower curve of the upper panel shows the residuals (offset by −0.8%) after fitting sinusoids at the frequencies indicated.

Comparing the flux and velocity Fourier Transforms, we note first of all, that the highest peak in Fourier Transform of the velocity curve coincides with the dominant peak in the Fourier transform of the light curve. Other such coincident peaks also seem to be present, albeit at a lower amplitude. Since the two peaks at $6651\,\mu$Hz and $6928\,\mu$Hz in Fig. A.1b are not present in the light curve (at amplitudes greater than $0.9 \pm 0.8\%$ and $0.6 \pm 0.8\%$ respectively), we surmise that they are due to noise.

Applying the external information available from the light curve to the velocity curve, we infer the line-of-sight velocities in HL Tau 76 by fixing the frequencies to those obtained from the light curve. The resulting values are listed in Table A.1.

In order to subject these velocity amplitudes to similar tests as described in Sect. 4.1, we carry out another Monte Carlo

[1] We remind the reader that the amplitude which a driven mode reaches is not expected to depend on temperature, but on resonance conditions with daughter modes; see Wu & Goldreich (2001).

Table A.1. Pulsation frequencies and other derived quantities from the light and velocity curves for HL Tau 76.

Mode	Period (s)	Frequency (μHz)	A_L (%)	Φ_L (°)	A_V (km s^{-1})	Φ_V (°)	R_V (Mm rad^{-1})	$\Delta\Phi_V$ (°)
Real Modes:								
F1	657	1521	3.3 ± 0.8	−57 ± 14	3.2 ± 1.0	34 ± 18	10 ± 4	91 ± 23
F2	597	1675	1.7 ± 0.8	−91 ± 28	0.3 ± 1.1	···	2 ± 6	···
F3	541	1848	5.6 ± 0.8	42 ± 9	4.0 ± 1.1	84 ± 15	6 ± 2	41 ± 18
F4	494	2023	2.6 ± 0.8	70 ± 19	3.7 ± 1.0	47 ± 16	11 ± 5	−24 ± 25
F5	383	2614	3.3 ± 0.8	25 ± 14	2.1 ± 1.0	144 ± 27	4 ± 2	118 ± 31
F6	781	1280	2.2 ± 0.8	−81 ± 22	3.1 ± 1.0	48 ± 19	18 ± 9	130 ± 29
Combinations:								
Mode	Period	Frequency	A_L	Φ_L	A_V	Φ_V	R_C	$\Delta\Phi_C$
F1+F3	297	3369.0	2.3 ± 0.8	−20 ± 20	1.4 ± 1.0	···	6 ± 3	−5 ± 26
F3+F6	320	3128.0	2.0 ± 0.8	−63 ± 24	0.7 ± 1.0	···	8 ± 5	−24 ± 33

Note. Quantities derived from the light and velocity curves with frequencies fixed to those listed in Dolez & Kleinman (1996) whose nomenclature we follow. $A_{L,V}$ and $\Phi_{L,V}$ are the amplitudes and phases obtained from fits to the light and velocity curves respectively. $R_V = A_V/(2\pi f A_L)$; $\Delta\Phi_V = \Phi_V - \Phi_L$. $R_C = A_L^{i\pm j}/(n_{ij}A_L^i A_L^j)$ here $n_{ij} = 2$. $\Delta\Phi_C = \Phi_L^{i\pm j} - (\Phi_L^i \pm \Phi_L^j)$ gives the relative phase of the combination mode with that of its constituent real modes.

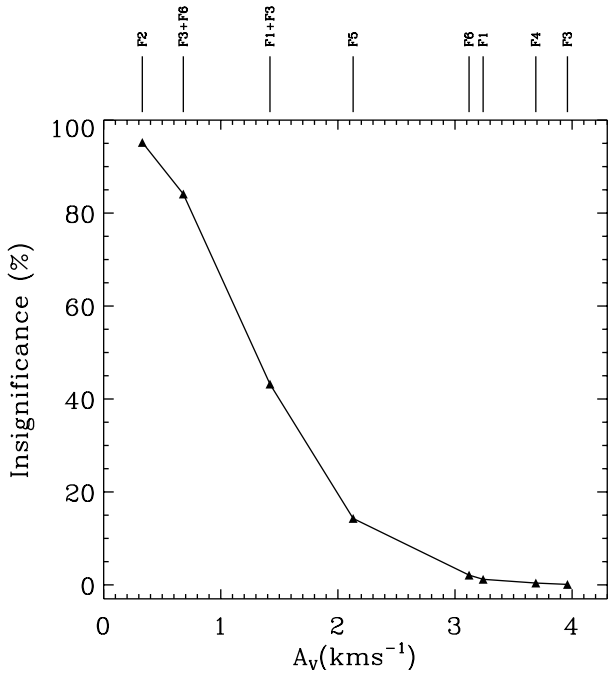

Fig. A.2. Results of the Monte Carlo simulation described in Appendix A i.e. fitting randomly shuffled velocity curves of HL Tau 76 with frequencies fixed to those obtained from the WET data. The triangles mark the velocity amplitudes thus derived. These amplitudes and their corresponding phases are listed in Table A.1. The figure shows that the signals at F3, F4, F1, and F6 are unlikely to be due to chance.

simulation, this time taking into account the external information available from the light curve. We fit the shuffled data sets with frequencies *fixed* to those observed in the light curve. Repeating this process 1000 times, we find that the peak in the velocity FT at F3 – the strongest mode in the light curve – now has a 0.1% chance of being a random peak. Clearly, this improvement cf. Table 2 is due to the imposition of additional information.

Following the notation of van Kerkwijk et al. (2000), we derive the relative velocity to flux amplitude ratios and phases, R_V and $\Delta\Phi_V$. The strongest mode, F3, has a period of 541 s that is intermediate between that of HS 0507+0434 (355 s, Jordan et al. 1998) and ZZ Psc (614 s, van Kerkwijk et al. 2000). The measured velocity amplitude at F3 also lies between that of HS 0507+0434 (2.6 ± 1.0 km s^{-1}, Kotak et al. 2002) and ZZ Psc (5.4 ± 0.8 km s^{-1}, van Kerkwijk et al. 2000). The values of R_V for all of the modes are consistent with each other and with having a spherical degree (ℓ) of 1. However, we note with interest that the one mode in ZZ Psc identified as having $\ell = 2$ by Clemens et al. (2000), was at a period of 776 s which is very close to the period of our F6. Even though the differences in R_V are not formally significant, that F6 has the largest R_V is consistent with it having a higher ℓ value, as flux variations for higher ℓ values suffer stronger cancellation while the line-of-sight velocities do not (e.g. van Kerkwijk et al. 2000). Comparison with the pulsation periods of ZZ Psc is justified; indeed, Dolez & Kleinman (1996) comment on the striking similarities in the modes observed for these two white dwarfs. A more definitive ℓ-identifcation might be possible from analysing the wavelength dependence of pulsation amplitudes or from a much longer time series which is able to resolve multiplets within a period group.

References

Beland, S., Boulade, O., & Davidge, T. 1988, CFHT Info. Bull., 19, 16
Bergeron, P., Wesemael, F., Lamontagne, R., et al. 1995, ApJ, 449, 258
Bohlin, R. C., Colina, L., & Finley, D. S. 1995, AJ, 110, 1316
Bradley, P. A. 1998, Balt. Astr., 7, 355
Brickhill, A. J. 1990, MNRAS, 246, 510
Brickhill, A. J. 1991, MNRAS, 251, 673

Clemens, J. C. 1993, Balt. Astr., 2, 407
Clemens, J. C., van Kerkwijk, M. H., & Wu, Y. 2000, MNRAS, 314, 220
Dolez, N., & Kleinman, S. J. 1996, White Dwarfs, ed. J. Isern, M. Hernanz, & E. Garcia-Berro (Kluwer), 429
Dolez, N., & Vauclair, G. 1981, A&A, 102, 375
Dziembowski, W., & Koester, D. 1981, A&A, 97, 16
Gautschy, A., Ludwig, H. G., & Freytag, B. 1996, A&A, 311, 493
Giovannini, O., Kepler, S. O., Kanaan, A., et al. 1998, Balt. Ast., 7, 131
Goldreich, P., & Wu, Y. 1999a, ApJ, 511, 904
Goldreich, P., & Wu, Y. 1999b, ApJ, 523, 805
Greenstein, J. L. 1982, ApJ, 258, 661
Horne, K. 1986, PASP, 98, 609
Jordan, S., Koester, D., Vauclair, G., et al. 1998, A&A, 330, 227
Kepler, S. O., Giovannini, O., Kanaan, A., et al. 1995, Balt. Astr., 4, 157
Koester, D., & Vauclair, G. 1996, White Dwarfs, ed. J. Isern, M. Hernanz, & E. Garcia-Berro (Kluwer), 429
Kotak, R., van Kerkwijk, M. H., & Clemens, J. C. 2002, A&A, 388, 219
Landolt, A. 1968, ApJ, 153, 151
Nather, R. E., Winget, D. E., Clemens, J. C., et al. 1990, ApJ, 361, 309
Oke, J. B., Cohen, J. G., Carr, M., et al. 1995, PASP, 107, 375
Robinson, E., Mailloux, T., Zhang, E., et al. 1995, ApJ, 438, 908
Stone, R. C. 1996, PASP, 108, 1051
van Kerkwijk, M. H., Clemens, J. C., & Wu, Y. 2000, MNRAS, 314, 209
Winget, D. E., van Horn, H. M., Tassoul, M., et al. 1982, ApJ, 252, L65
Wu, Y., & Goldreich, P. 1999, ApJ, 519, 783
Wu, Y., & Goldreich, P. 2001, ApJ, 546, 469